8. A. J. Gotch and T. S. Zwier, *J. Chem. Phys.* **96**, 3388 (1992).
9. See, for example, R. Mahon, T. J. McIlrath, V. P. Myerscough, D. W. Koopman, *IEEE J. Quantum Electron.* **QE-15**, 444 (1979).
10. K. W. Chang and W. R. M. Graham, *J. Mol. Spectrosc.* **94**, 69 (1982); H.-J. Haink and M. Jungen, *Chem. Phys. Lett.* **61**, 319 (1979).
11. S. G. Lias, J. E. Bartmess, J. L. Holmes, R. D. Levin, W. G. Mallard, *J. Phys. Chem. Ref. Data* **17**, 82 (1988).
12. This work was supported by the National Aeronautics and Space Administration Planetary Atmospheres Program.

28 July 1992; accepted 2 October 1992

Production and Initial Characterization of Bionites: Materials Formed on a Bacterial Backbone

Neil H. Mendelson

The addition of soluble metal salts of calcium, iron, or copper to cultures of *Bacillus subtilis* grown in web form nucleated precipitation at the surface of the bacterial cell walls. The mineralized cell filaments can be drawn into a fiber that when dried consists of a bacterial thread backbone carrying an inorganic solid. The ratios of organic to inorganic components (by weight) in the stiff brittle materials, called bionites, were: 1.08 for fe(2)bactonite, 1.8 for calbactonite, 2.3 for fe(3)bactonite, and 5 for cu(2)bactonite. X-ray photoelectron spectra suggest that the fe(3)bactonite contains Fe_2O_3, that calbactonite contains calcium carbonate, and that cu(2)bactonite contains CuCl (Cu I). Acid-base reactions of the bionites are compatible with these identifications. Burning out the organic phase of the febactonites yields a black magnetic material, presumably magnetite. The burnt cubactonite appears to yield elemental Cu(s). Calbactonite upon hydration was able to retain a genetically engineered enzymatic activity.

Recent advances in biotechnology have provided new tools for the manipulation of biological materials and the production of chemical products (*1*). Similar approaches have yet to be applied to materials synthesis. This report describes a system in which it may be possible to do so. The basic idea is to use bacterial cell walls in situ as a matrix for mineralization and to draw the products (*2*) into fiberlike materials. Three such products, called bionites, are described here: (i) calbactonite, a calcium material; (ii) febactonites, which are iron derivatives; and (iii) cubactonites, which are copper derivatives. All three forms were produced on *Bacillus subtilis* strains shown previously to be suitable for drawing into threadlike fibers. The electronegative nature of the cell wall in vivo is the basis for metal binding.

The *B. subtilis* cell wall is a gel-like viscoelastic material composed primarily of two polymers: peptidoglycan and teichoic acid (*3*). Both carry ionizable groups that have the potential for metal binding (*4*). Carboxylate groups in the peptide moiety of peptidoglycan are believed to be the primary sites of metal binding (*5*). Cell walls behave as complex ion exchangers. Some bacterial walls have capacities (3.5 milliequivalents per gram) that are equivalent to those of commercial resins such as Dowex A-1 (*6*). Although there is selectivity in the binding of counterions in vivo, cell walls are capable of binding many different ions (*4*, *6*, *7*). Ions such as Fe^{3+}, Cu^{2+}, and Ca^{2+} are known to bind in high quantities (*4*). In living cells, the wall is a multilayered material that is cross-linked into a supramolecular network that encompasses the entire cell (a cylindrical shape about 4 μm long by 0.7 μm in diameter). The *B. subtilis* cell wall is a dynamic structure that is constantly added to on the inner surface and shed on the outside (*8*). The material itself is a flexible porous network of considerable strength (*2*).

The bionites were produced by using derivatives of *B. subtilis* strain FJ7 called 7(II), 7(O), and F3N. The first two strains have been selected for their ability to grow as web cultures from which bacterial threads of uniform diameter can be drawn (*9*). The genetically engineered strain F3N carries the *Escherichia coli* lacZ gene under the control of an unidentified host gene promoter and constitutively produces the enzyme β-galactosidase (*10*). It can also be grown in web form but not as successfully as those selected for that property. Web cultures were grown at 20°C in TB medium (*11*) for ~18 hours. One milliliter of 0.5 M $CaCl_2$, 1 M $FeCl_3$, or 1 M $CuCl_2$ was added to each web culture and dispersed, taking care not to disrupt the integrity of the web. The mixtures were incubated at 23°C for periods indicated in each experiment described below. The mineralized web (Fig. 1, A and B) was then drawn into the room atmosphere at the rate of 5 mm/min with a rate-controlled electric motor (Fig. 1, C to E). The drawing process itself compressed the adherent wet precipitate along with the cellular filaments at the fluid-air interface. The draw rate was chosen to prevent the weight of the wet fiber from exceeding the tensile strength of the bacterial filaments, which is inversely related to their water content. The wet fibers were hung vertically and allowed to dry. Additional fluid drained from them during this process. In

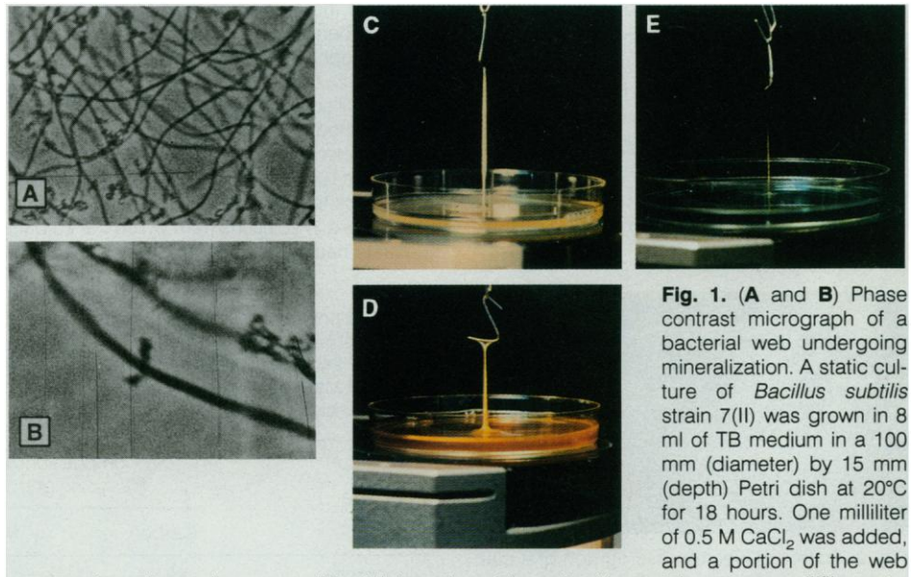

Fig. 1. (**A** and **B**) Phase contrast micrograph of a bacterial web undergoing mineralization. A static culture of *Bacillus subtilis* strain 7(II) was grown in 8 ml of TB medium in a 100 mm (diameter) by 15 mm (depth) Petri dish at 20°C for 18 hours. One milliliter of 0.5 M $CaCl_2$ was added, and a portion of the web was transferred to a microscope slide. (A) A portion of the web with crystals on some cell filaments. (B) A higher magnification view of a single filament with crystals aligned perpendicular to the filament axis. Filament diameter in both is 0.7 μm. (**C** to **E**) Bionites being drawn from mineralized webs of *B. subtilis*. Fibers were drawn after 1 hour of mineralization of web cultures with (C) $CaCl_2$, (D) $FeCl_3$, and (E) $CuCl_2$. Draw rate was 5 mm/min. Petri dish diameter is 100 mm.

Department of Molecular and Cellular Biology, University of Arizona, Tucson, AZ 85721.

the dried bionite fiber, the cellular filaments are aligned parallel to the fiber axis as they are in standard bacterial thread.

The average metal content of each bionite and the binding energy peaks obtained by x-ray photoelectron spectroscopy (XPS) from pooled fibers are shown in Table 1. These spectra (1000 to 0 eV) indicate that calbactonite contains calcium carbonate, fe(3)bactonite contains Fe_2O_3 (hematite, or maghemite, or both), and cu(2)bactonite contains CuCl as the mineral components. The spectra also revealed the presence of sodium, chlorine, nitrogen, and oxygen in all three bionites (carbon could not be measured because of its presence in the tape to which the specimens were attached). These other elements reflect the bacterial component and the high concentration of salt in the growth medium within which the bionites were produced. In addition, a small amount of phosphorus was detected in calbactonite and a small amount of silicon was detected in cu(2)bactonite.

The wet calbactonite fiber after drawing is a pliable white to gray-white material that, depending on the conditions of the web culture from which it is made, can reach 12 cm in length by 2 mm in diameter. The fiber shrinks 30 to 40% in length upon drying. When dried to ambient conditions, a brittle, rigid material that cracks predominantly perpendicular and parallel to the fiber axis is formed (Fig. 2). Examination of crack edge cross sections indicates mineralization in granular form throughout the entire material. Upon hydration, the material swells and becomes pliable again, but the individual cellular filaments remain intact even when subjected to a flow rate in the range of 0.01 to 10 ml/min. When hydrated, calbactonite produced from strain F3N carries an immobilized β-galactosidase activity. The white fiber turns blue when incubated in the chromogenic substrate X-gal. Enzyme activity can be measured with *o*-nitrophenyl-β-D-galactopyranoside (Sigma, St. Louis, Missouri) as substrate and by determining the absorbance at 420 nm (A_{420}) of the suspension (Fig. 3). The enzyme activity is not released from the fiber during the course of the reaction. Calbactonite from which the carbon has been burned out has no activity with either substrate.

Fe(3)bactonite initially drawn as a white-tan wet fiber dries to a red-orange material (Fig. 4A). In the cone formed at the fluid-air interface, bundles of cell filaments are evident, indicating cross-linking of the filaments in the web. These bundles can also be seen as substructure in the dry bionite. Cross-linking stabilizes the fiber during production. Fibers 10 cm or longer are readily obtained even from webs of poor quality that contain cell filaments shorter than those shown in Fig. 1, A and B. The dried fibers spontaneously develop surface cracks primarily perpendicular to the fiber axis. The plates produced by cracking are aligned along the fiber axis with the cellular filaments, suggesting that the bacterial wall matrix influences the order of the mineral phase. An edge cross section (Fig. 4B) reveals mineralization throughout with material coating individual cell filaments. Many specimens form fine, whisker-like projections from their surfaces (Fig. 4C). Although fe(3)bactonite fibers do not appear to respond to a magnetic field, burning out their organic material yields a black magnetic material, presumably magnetite. Fe(3)bactonite fibers exposed to acid (pH < 2) swell initially as in water and then separate into individual cellular filaments. In base (pH > 10), they swell to form a deep red-orange material that is spongy but brittle.

Cu(2)bactonite drawn from a web to which $CuCl_2$ was added (giving rise to a blue solution of hydrated cupric ion) begins as a white fiber but quickly darkens to a green-silver material (Fig. 5A) as it dries. The color suggests that a coating of copper hydroxy carbonate may form. CuCl, identified by XPS as the major material, is a white solid. Cu(2)bactonite fibers are characteristically thin (~100-μm diameter) and long, much like their standard bacterial thread counterparts. Incubation for 1 hour in copper yields a fiberglass-like material within which flecks of deposited metal can be seen as isolated islands, whereas a similar exposure to either calcium or iron results in a fully mineralized fiber. More heavily loaded copper fibers can be produced, however, by longer incubations. What appears to be elemental copper can be recovered from such fibers by burning away the carbon (Fig. 5B). Cu(2)bactonite fibers swell when hydrated at neutral, acidic, or basic pH. In base, they immediately turn a pink-purple color that persists even though the fiber swells into a translucent rubbery gel-like

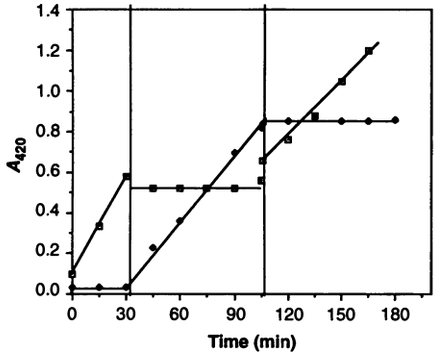

Fig. 3. β-Galactosidase immobilized enzyme activity. Calbactonite produced on *B. subtilis* strain F3N was immersed in distilled water for 1 min at 23°C and redrawn. A 6.7-mg piece of the dried bionite was transferred to 4 ml of 1 mg/ml *o*-nitrophenyl-β-D-galactopyranoside in Z-buffer (*21*), and the mixture was incubated at 37°C (flask 1, open squares). A second flask containing *o*-nitrophenyl-β-D-galactopyranoside in Z-buffer without calbactonite was also incubated (flask 2, filled symbols). The A_{420} was determined periodically. After 30 min of incubation, the calbactonite was transferred from flask 1 to flask 2. At 106 min, the calbactonite was transferred back to flask 1. No enzyme activity could be detected in solutions from which the calbactonite was removed. The second transfer shows that substrate had not been exhausted during the initial incubation in flask 1.

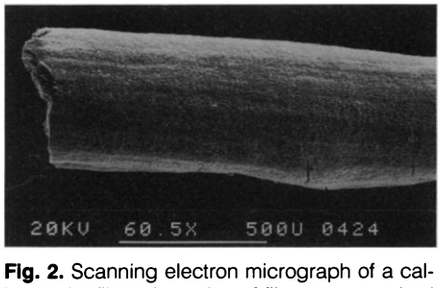

Fig. 2. Scanning electron micrograph of a calbactonite fiber. A section of fiber was attached to an aluminum stub with double stick tape, coated with gold, and examined with an ISI model DS-130 scanning electron microscope. Bar = 500 μm.

Table 1. Bionite composition. Percent by weight of carbon and metals was determined from pooled samples of bionites of each class produced after 1 hour of exposure to the metal ion. (Analysis by Galbraith Laboratories, Knoxville, Tennessee). The XPS spectra (*20*) were obtained with an ESCALAB Mark II instrument at the University of Arizona Laboratory for Electron Spectroscopy and Surface Analysis.

Bionite	Composition (% by weight)		XPS peak binding energy (eV)	Comments
	Carbon	Metal		
Calbactonite	18.57	10.30	358.2*	$CaCO_3$
Fe(2)bactonite	17.10	15.75		
Fe(3)bactonite	22.67	9.70	731.2†	Fe_2O_3
Cu(2)bactonite	33.40	6.61	960.4‡	CuCl

*Ca $2p^{3/2}$. †Fe $2p^{3/2}$. ‡Cu $2p^{3/2}$; Auger parameter, 1847.6 eV.

material. If redrawn and dried, the gel collapses to a solid dark-purple crystalline material.

A study of the material properties of bionite fibers has been initiated with an instrument designed and built to measure bacterial thread and the test protocols used in their study (*12*). When measured in the direction of the fiber axis, bionites show much less variation in behavior with changes in relative humidity than do nonmineralized threads. For example, the tensile (Young's) modulus decreases by a factor of ~4 between 40 and 70% relative humidity, whereas the reduction for nonmineralized threads is ~20 times. However, at a given relative humidity, there is a substantial reduction in modulus as specimen diameter increases. The measured bionite mechanical properties appear to depend only to a small extent on the mineral component. For cubactonites, the tensile modulus of the mineral component is ~0.1 GPa compared with 12.6 GPa for dry bacterial wall (*2*).

A number of related bionites have been produced including fe(2)bactonite, a cubactonite generated with copper sulfate rather than copper chloride, and hybrid materials containing both copper and iron. Several principles are involved in the construction of all of the materials described here. First, the matrix upon which mineralization occurs is a complex polymeric material (Gram + bacterial cell wall) that carries charged groups distributed according to the molecular organization of the wall. Although the details of wall polymer organization are not currently understood, there is evidence that they are highly ordered but not crystalline in nature (*2*). The wall behaves as a complex ion exchanger that preferentially binds certain ions but that can bind many others. The chemical process giving rise to mineralization appears to be similar to those governing epicellular geochemical deposition nucleated on bacterial walls (*13*). In bionite production, however, these processes occur rapidly and at low temperatures (20° to 25°C). There are two phases to the process, an aqueous one in which a high concentration of ion is introduced, giving rise to precipitation at the cell surface, followed by dehydration. The entire process can be completed in less than 2 hours. The resulting bionites are suitable for further chemical or physical processing.

The bionite system provides biotechnological opportunities to manipulate materials synthesis because: (i) the organization of the bacterial cell wall can be controlled by genetic and physiological means (*14*), (ii) walls carry reactive groups that are suitable for mineral deposition as well as covalent linkage of various groups (*15*), and (iii) the bacterial thread system provides a means to draw the products into fibers (*9*). Calbactonite, febactonites, and cubactonites illustrate that diverse materials can be made with very different potential applications. The calcified bionite that carries calcium carbonate can be used as an immobilized cell-enzyme system (*16*). In some ways, the material may resemble the calcite and aragonite found in marine chalk deposits thought to be nucleated by bacteria (*17*). Calcium phosphates are also known to become deposited on bacterial cells. These are of interest in view of their relation to bone (*17*). Whether a hydroxylapatite bionite can be made remains to be determined, however. The iron bionites provide a potential new route for making materials with unusual magnetic or optical properties such as the nanocrystalline maghemite form recently described (*18*). The bionite system also provides opportunities to study the mineralization process itself of interest in geochemistry, biology, and in the biomimetic production of new composite materials (*19*).

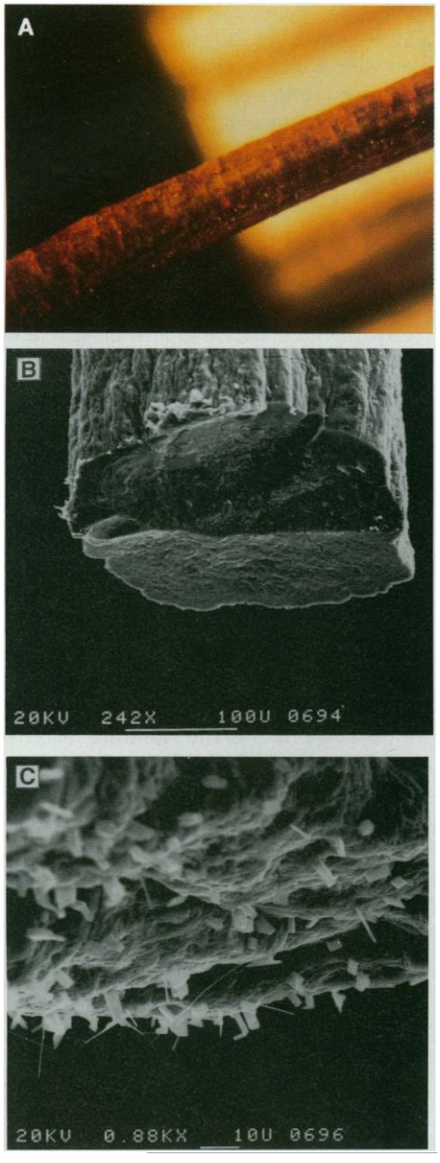

Fig. 4. (**A**) Surface appearance of fe(3)bactonite. The photograph was taken with lighting from above through an Olympus stereoscopic microscope. Fiber diameter is ~0.5 mm. (**B**) Fe(3)bactonite structure. Scanning electron micrograph of a cross section showing both interior and surface details. Mineralization throughout is evident. Bar = 100 μm. (**C**) Surface whiskers on fe(3)bactonite. Scanning electron micrograph of the bionite surface showing crystals and whiskers as well as the amorphous mineralization on cellular filaments throughout. The fiber axis runs horizontally in the figure. Bar = 10 μm.

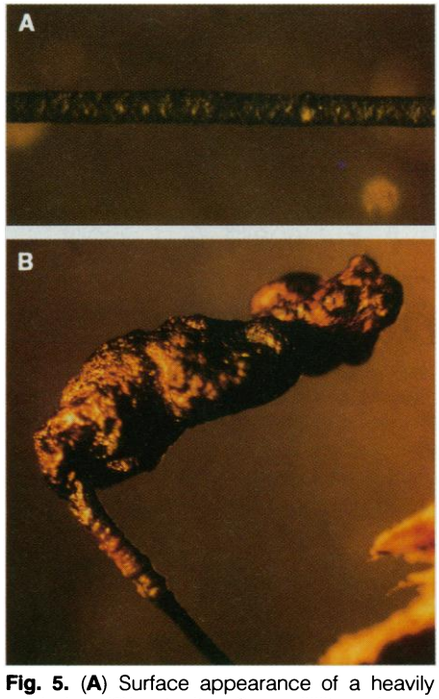

Fig. 5. (**A**) Surface appearance of a heavily loaded cu(2)bactonite. One milliliter of 1 M $CuCl_2$ was added to an 8 ml web culture of strain 7(II), and the mixture was incubated for 102 min at 23°C. The fiber was drawn in room atmosphere and allowed to dry. The photograph was taken with lighting from above through an Olympus stereoscopic microscope. Fiber diameter is ~125 μm. (**B**) Cu(2)bactonite residue after burning. Part of a fiber was ignited by passing through a Bunsen burner flame. The portion ignited burned with a blue flame. The transition zone between the burned portion and the initial fiber is shown. The green-black fiber yields an orange material that resembles elemental copper. (The material in the lower right of the figure is mounting tape.) The preburned fiber diameter was ~125 μm.

REFERENCES AND NOTES

1. See, for example, P. H. Abelson, *Science* **219**, 611 (1983); D. E. Koshland, Jr., *ibid.* **252**, 1593 (1991).

2. J. J. Thwaites and N. H. Mendelson, *Adv. Microb. Physiol.* **32**, 173 (1991).
3. T. J. Beveridge, in *Metal-Microbe Interactions*, R. K. Poole and G. M. Gadd, Eds. (IRL Press, New York, 1989), pp. 65–83.
4. _____ and R. G. E. Murray, *J. Bacteriol.* **127**, 1502 (1976).
5. R. J. Doyle, in *Metal Ions and Bacteria*, T. J. Beveridge and R. J. Doyle, Eds. (Wiley, New York, 1989), pp. 275–293.
6. R. E. Marquis, K. Mayzel, E. L. Carstensen, *Can. J. Microbiol.* **22**, 975 (1976).
7. M. N. Hughes and R. K. Poole, *Metals and Microorganisms* (Chapman & Hall, New York, 1989), p. 337.
8. H. M. Pooley, *J. Bacteriol.* **125**, 1127 (1976); *ibid.*, p. 1139; J. Chaloupka, L. R. Kreckova, P. Kreckova, *Folia Microbiol. (Prague)* **9**, 9 (1964).
9. J. J. Thwaites and N. H. Mendelson, *Proc. Natl. Acad. Sci. U.S.A.* **82**, 2163 (1985).
10. B. Salhi, thesis, University of Arizona, Tucson (1991).
11. N. H. Mendelson, *Proc. Natl. Acad. Sci. U.S.A.* **73**, 1740 (1976).
12. _____ and J. J. Thwaites, *J. Bacteriol.* **171**, 1055 (1989).
13. S. Mann, in *Biomineralization in Lower Plants and Animals*, B. S. C. Leadbeater and R. Riding, Eds. (Clarendon, Oxford, 1986), pp. 39–45; see also W. E. Krumbein, *ibid.*, pp. 55–72; F. G. Ferris, W. S. Fyte, T. J. Beveridge, *Geology* **16**, 149 (1988).
14. N. H. Mendelson, *Sci. Prog.* **74**, 425 (1990); in *Microbiology—1977*, D. Schlessinger, Ed. (American Society for Microbiology, Washington, DC, 1977), pp. 5–24.
15. T. J. Beveridge and R. G. E. Murray, *J. Bacteriol.* **141**, 876 (1980).
16. H. E. Swaisgood, in *Enzymes and Immobilized Cells in Biotechnology*, A. Laskin, Ed. (Benjamin/Cummings, Menlo Park, CA, 1985), pp. 1–24; G. C. Guilbault, *Analytical Uses of Immobilized Enzymes* (Dekker, New York, 1984).
17. F. G. E. Pautard, in *Biological Calcification*, H. Schraer, Ed. (North-Holland, Amsterdam, 1970), pp. 106–201; R. Y. Morita, *Geomicrobiol. J.* **2**, 63 (1980).
18. R. F. Ziolo *et al.*, *Science* **257**, 219 (1992).
19. A. H. Heuer *et al.*, *ibid.* **255**, 1098 (1992); P. Calvert and S. Mann, *J. Mater. Sci.* **23**, 3801 (1988).
20. P. G. Rouxhet and M. J. Genet, in *Microbial Cell Surface Analysis: Structural and Physico-Chemical Methods*, N. Mozes, P. S. Handley, H. J. Busscher, P. G. Rouxhet, Eds. (VCH, New York, 1991), pp. 173–220.
21. J. H. Miller, *Experiments in Molecular Genetics* (Cold Spring Harbor Laboratory, Cold Spring Harbor, NY, 1972).
22. Supported in part by grants from the National Institute of General Medical Sciences, the University of Arizona and the Arizona Agricultural Experiment Station and a contract from the Air Force Office of Scientific Research. I am indebted to K. W. Nebeshy for XPS measurements, P. D. Calvert for numerous suggestions and guidance, J. J. Thwaites for fiber mechanics measurements, and S. D. Whitworth and H. Fisher for excellent technical assistance.

4 August 1992; accepted 19 October 1992

Electrical Resistivity and Stoichiometry of Ca_xC_{60} and Sr_xC_{60} Films

R. C. Haddon, G. P. Kochanski, A. F. Hebard, A. T. Fiory, R. C. Morris

The temperature- and concentration-dependent resistivities of annealed Ca_xC_{60} and Sr_xC_{60} films were measured near room temperature. Resistivity minima were observed at $x = 2$ and 5. The resistivities of these films were $\rho_{min} \sim 1$ ohm-centimeter for $x = 2$ and $\rho_{min} \sim 10^{-2}$ ohm-centimeter for $x = 5$. This latter value is comparable to the resistivities found in similar experiments on K_3C_{60} films. There is a maximum in the resistivity between $x = 2$ and 3, and another at $x \sim 7$. The conductivity is activated over the whole range of compositions, and the activation energy scales with the logarithm of the resistivity. The results suggest that the conductivity and superconductivity observed in Ca_5C_{60} are associated with the population of bands derived from the t_{1g} level of C_{60}.

Solid C_{60} and C_{70} undergo doping with alkali metals to produce conductors (*1*). For A = K or Rb, the A_3C_{60} phases are superconductors (*2–5*). It has been shown that Ca intercalates into the C_{60} face-centered-cubic lattice to form a solid solution and that a phase transformation occurs near a Ca/C_{60} ratio of 5/1 to produce a simple cubic structure that is a superconductor with a superconducting transition temperature $T_c = 8.4$ K (*6*). Photoemission studies indicate that C_{60} films lead to a metallic state on exposure to Sr vapor (*7*). Insofar as we are aware, no studies have reported on the transport properties of these systems. We present here resistivity measurements of Ca_xC_{60} and Sr_xC_{60} films, as a function of temperature and doping. We find that Ca- and Sr-doped C_{60} films show a resistivity profile that is entirely different from that observed on doping with alkali metals (*1*, *8*). The results suggest that the conductivity and superconductivity observed in Ca_5C_{60} are associated with the population of bands derived from the t_{1g} level of C_{60}. This implies that the most conducting state of the alkaline earth–doped phases arises from C_{60}^{z-} molecules with $6 > z > 12$, perhaps hybridized with Ca states.

We followed the general scheme adopted to study K_xC_{60} films in ultrahigh vacuum (UHV) (*8*), but there were important improvements in the experimental procedure. The UHV chamber used in this work was equipped with a Radak I evaporation source (Luxel Corporation) so that the C_{60} films were grown in situ and were not exposed to O_2 before doping. Results in the literature suggest that exposure of C_{60} films to O_2 leads to changes in the Raman spectrum (*9*), although the exact nature of this effect remains to be clarified. Furthermore, this modification allowed us to establish that the doped films were equilibrated under the conditions of our experiment by subsequent addition of C_{60} to Ca_xC_{60} films. The C_{60} films were grown from material produced in the spark erosion process (*10*) and purified by liquid chromatography (*11*). Films produced in this way consist of random polycrystalline grains of dimension ~60 Å (*12*). The Ca and Sr were deposited by thermal evaporation of the pure metal from a tungsten wire basket (R. D. Mathis Company). The UHV chamber also contains a quartz crystal microbalance so that we could directly monitor the amounts of C_{60} and metal that were deposited. The system was baked before deposition, and the base pressure was below 10^{-8} torr.

In the case of K doping the conductivity responded immediately to the addition of metal to the film (*9*), whereas in the present study a high-temperature anneal was necessary to equilibrate the system and obtain meaningful resistivities. We used thin C_{60} films (100 to 500 Å), in order to reduce the time required for the system to reach equilibrium. The electrical measurements were made with substrates similar to those described previously (*9*), except that we used sapphire as the substrate material and evaporated Al and Ag multilayers for contact pads. The quartz crystal microbalance was calibrated with Rutherford backscattering (RBS) measurements on a C_{60} film grown on clean hydrogen-terminated Si. Ex situ RBS analysis of the Ca and Sr peaks in the doped C_{60} films when combined with the C_{60} determination from the microbalance gave us the film composition. Results obtained at intermediate doping levels confirmed the linearity of the response of the quartz microbalance with deposition, and thus the measurements from the quartz microbalance can be used to obtain the film composition at each resistance determination. We estimate the uncertainty in our derived values of x at ±0.3, due mainly to nonuniformities in the metal sources and the error in the RBS measurements on thin metal/C_{60} films.

After a number of trial experiments, we used a 1-min anneal at 180°C to equilibrate Ca and Sr in the C_{60} film. With lower temperature anneals (down to 100°C), we obtained essentially the same behavior but the features observed in the resistivity were less distinct. At temperatures above 200°C, there was an increase in the contact resis-

AT&T Bell Laboratories, Murray Hill, NJ 07974.